

# qAttCNN - Self Attention Mechanism for Video QoE Prediction in Encrypted Traffic

Michael Sidorov and Ofer Hadar

January 13, 2026

## Abstract

The rapid growth of multimedia consumption, driven by major advances in mobile devices since the mid-2000s, has led to widespread use of video conferencing applications (VCAs) such as Zoom and Google Meet, as well as instant messaging applications (IMAs) like WhatsApp and Telegram, which increasingly support video conferencing as a core feature. Many of these systems rely on the Web Real-Time Communication (WebRTC) protocol, enabling direct peer-to-peer media streaming without requiring a third-party server to relay data, reducing the latency and facilitating a real-time communication. Despite WebRTC's potential, adverse network conditions can degrade streaming quality and consequently reduce users' Quality of Experience (QoE). Maintaining high QoE therefore requires continuous monitoring and timely intervention when QoE begins to deteriorate. While content providers can often estimate QoE by directly comparing transmitted and received media, this task is significantly more challenging for internet service providers (ISPs). End-to-end encryption, commonly used by modern VCAs and IMAs, prevent ISPs from accessing the original media stream, leaving only Quality of Service (QoS) and routing information available. To address this limitation, we propose the QoE Attention Convolutional Neural Network (qAttCNN), a model that leverages packet size parameter of the traffic to infer two no-reference QoE metrics viz. BRISQUE and frames per second (FPS). We evaluate qAttCNN on a custom dataset collected from WhatsApp video calls and compare it against existing QoE models. Using mean absolute error percentage (MAEP), our approach achieves 2.14% error for BRISQUE and 7.39% for FPS prediction.

**Keywords** — Quality of Experience in Video, Encrypted Traffic, Multi-headed Self-attention, Deep Learning, Machine Learning, Video Conferencing

## 1 Introduction

Predicting the Quality of Data (QoD) delivered to the end user is a central challenge in modern communication systems, as it directly shapes users' Quality of Experience (QoE). QoE, in turn, strongly influences whether users continue using (or abandon) a specific Content Provider (CP) or Internet Service Provider (ISP).

The most direct way to assess QoD (and consequently QoE) is to compare, at the client side, the received content with the original data transmitted by the server. In practice, however, such end-to-end comparison is feasible primarily for CPs, since they control both ends of the delivery pipeline. For ISPs to obtain similar insight, they would need to intercept and analyze transferred packets, a practice historically known as Deep Packet Inspection (DPI), which was widely used during the 1990s and early 2000s.

Since approximately 2010, the rapid growth of the internet and increased privacy concerns have made end-to-end encryption a fundamental requirement for most online communications. As a result, traditional DPI has become largely ineffective for ISPs [19], because encrypted traffic payloads cannot be interpreted without access to private keys.

Consequently, ISPs must rely primarily on passive measurements of the network Quality of Service (QoS) [8]. Their objective is to infer QoD from observed QoS metrics, and ultimately predict users' QoE. This inference is inherently challenging due to the complex and highly non-linear relationship between QoS and QoE, motivating extensive research over the past decades.

For high-volume applications such as video streaming, a data-driven approach particularly natural. Accordingly, numerous machine learning (ML) and deep learning (DL) methods have been proposed to infer QoE under encrypted traffic constraints, achieving progressively improved accuracy.

The remainder of this paper is organized as follows. Section 2 surveys recent studies on QoE prediction and highlights works using attention mechanisms to improve performance across domains. Section 3 analyzes the dataset used in our experiments. Section 4 presents the proposed method, and Section 5 describes the experiment setup employed during models' performance

evaluation. Section 6 reports the experimental results, and finally, Section 7 concludes the paper, discusses limitations, and outlines directions for future research.

## 2 Related Work

The domain of QoE analysis has been extensively studied over the years. Bentaleb et al. [2] introduced a Recursive Least Squares (RLS) model to predict the instantaneous available network bandwidth. Their goal was to improve QoE by optimizing the data chunk size within the Dynamic Adaptive Streaming over HTTP (DASH) protocol. Through their method, the authors reported improved achieved bitrates and a reduction in stall events during video streaming sessions.

Numerous studies have proposed Neural Network (NN) and Deep Learning (DL)-based methods for QoE prediction under the constraint of encrypted traffic. For example, Vega et al. [33] introduced an unsupervised DL model based on a Restricted Boltzmann Machine (RBM) [10] for real-time prediction of various No-Reference (NR) QoE metrics in video streaming. Their model estimates indicators such as video jerkiness, image blockiness, and multiple blur and noise related features. Although they report an accuracy exceeding 85%, this performance is achieved only for a specific type of video content, limiting the generalization of their approach.

Raca et al. [23] explored two classical ML methods, viz. Support Vector Machines (SVM) and Random Forests (RF), alongside a DL approach using Long Short-Term Memory (LSTM) networks to predict throughput in cellular networks. Their experiments demonstrated that increasing the granularity of the input data improved performance, reflected in a reduced absolute error percentage between predicted and actual throughput.

A Reinforcement Learning (RL)-based framework was proposed by Mao et al. [18], which computes three QoE metrics using predicted values of bitrate, available bandwidth, and buffer level in video sessions. Their results show that the RL model significantly outperforms traditional Adaptive Bitrate (ABR) mechanisms for QoE optimization.

The self-attention mechanism has found broad applicability across domains ranging from genetics to municipal operations. Following the breakthrough success of Transformers in Natural Language Processing (NLP) [34] and their subsequent adoption in computer vision tasks [7], consider-

able research has focused on incorporating attention, particularly multi-head self-attention, into various deep learning architectures (e.g., CNNs, RNNs, LSTMs). These hybrid models often achieve substantial performance gains by enhancing the expressiveness of the most relevant features while suppressing those with minimal impact on the predicted variable.

Building on similar ideas, Zhao et al. [38] proposed an attention-enhanced model augmented with a Sparrow Search Algorithm (SSA) to mitigate accuracy degradation caused by outliers. Their approach was applied to electricity price prediction in energy markets and demonstrated improved robustness and forecasting performance.

Liu et al. [15] developed a hybrid architecture combining CNN, attention (ATT), and LSTM modules to estimate carbon emission levels using features spanning the economic, societal, energy, and environmental domains. Their experiments demonstrated clear performance improvements attributable to the inclusion of the attention mechanism.

Another study, combining CNN, LSTM, and attention modules, was conducted by Liu et al. [14], who proposed a method for total electron content (TEC) prediction in the ionosphere, i.e., the electrically charged layer of the atmosphere. Their model, termed Att-CNN-BiLSTM, extends earlier work by Tang et al. [32] by replacing the previously used unidirectional LSTM with a bidirectional LSTM (BiLSTM). In their approach, the CNN extracts positional features, while the BiLSTM captures temporal dependencies. These complementary representations are then adaptively weighted by an attention mechanism, resulting in accurate predictions of TEC values.

Yi et al. [36] proposed a composite model consisting of an attention module (Att), a convolutional network (CNN), and a temporal convolutional network (TCN) for process quality prediction in an industrial setting. Their system successfully predicted the final quality of silk-weaving processes in Yuxi City, Yunnan Province, China. The dataset included 14,100 one-second interval measurements (such as ambient temperature, humidity, and compressed air pressure), used to predict two key quality indicators: outlet temperature and outlet moisture. Their method achieved superior predictive accuracy compared to traditional baselines.

### 3 Data

In the present study, we used the same dataset as in [29]. This dataset was collected in a controlled environment simulating a WhatsApp video call between two users — one using a smartphone and the other a laptop. Using the Wireshark application, we captured the state of the data line, including various features related to both the line itself and the traffic traversing it; these features are listed in table 1. The final dataset contains 51,341 entries, each corresponding to aggregated measurements over a 1-millisecond interval recorded during the WhatsApp video session.

Table 1: Description of that features that were recorded on the line between the two participants in a IMVCA session.

Feature	Data Type
The arrival time of the current frame	<i>float64</i>
The time passed since the start of the current time epoch	<i>float64</i>
The source IP address of the packet	<i>str</i>
The destination IP address of the packet	<i>str</i>
The protocol of the IP packet	<i>float64</i>
The length of the IP packet	<i>float64</i>
The source port of the UDP datagram	<i>int64</i>
The destination port of the UDP datagram	<i>int64</i>
The length of the UDP datagram	<i>int64</i>

Inspired by the successful use of micro-scale features in [27], given that such features are straightforward to extract, as they correspond to direct measurements of the line state (which also facilitate a real-time applications), and as it was previously shown that packet size is one of the strongest predictors in problems concerning encrypted traffic [20, 22, 6, 3, 9, 21, 26], in our current work, we have chosen to use the instantaneous packet size (PCKT) of the data traversing the line as the primary feature for predicting the QoE metrics, viz. BRISQUE and FPS, as summarized in table 2.

#### 3.1 Exploratory Data Analysis (EDA)

In this subsection we explore the properties of the dataset used in this study, and elaborate on the decisions made in the process of model design and

Table 2: In this table presented the features used in our experiments, i.e., only the total number of packets traversing the line in intervals of 1 millisecond

Feature Name	Data Type	Description
packet_size_1	int16	Number of arriving packets in the first time interval
packet_size_2	int16	Number of arriving packets in the second time interval
packet_size_3	int16	Number of arriving packets in the third time interval
...	...	...
packet_size_350	int16	Number of arriving packets in the last time interval

training.

### 3.1.1 Features

We examined the micro-level packet size features for cross-correlation, and found that they are largely uncorrelated, with the exception of the last 80 features ( $pckt_{270}$  —  $pckt_{350}$ ), as shown in fig. 1 (left). We hypothesize that this behavior arises from inherent properties of the dataset, which exhibit a significant degree of non-stationarity across samples, as discussed in section 3.1.3.

### 3.1.2 Labels

The distribution of BRISQUE labels exhibit a mixture of two gaussian distribution, with two means — one near 50 and another around 80 (fig. 2 left). This non-uniformity suggests that models may struggle to accurately learn and predict traffic associated with BRISQUE values in the intermediate range of 50-80. A similar pattern is observed in the FPS labels: the majority of samples correspond to medium level of FPS, viz. 20, while much smaller number of samples lay below or above it.

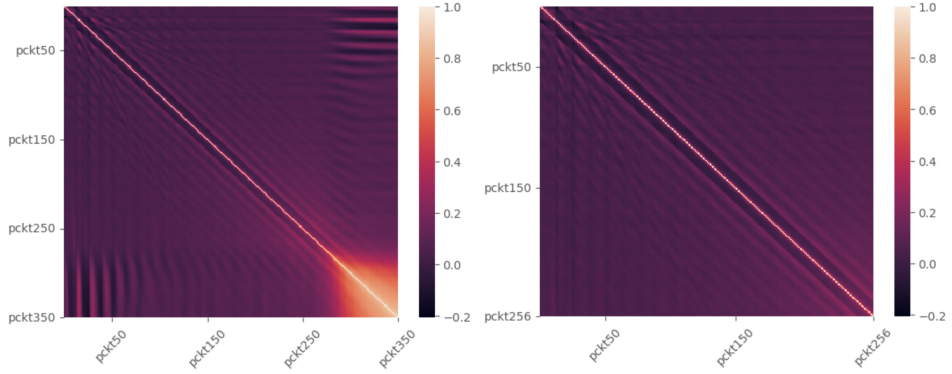


Figure 1: Left - Correlation heatmap of the full data packet size features used for prediction. Right - Correlation heatmap of the truncated dataset with 256 first packet sizes (i.e., excluding the non-stationary data tail). The  $pckt_\tau$  for  $\tau = 1, 2, \dots, 350$  represents the size of the packet in time interval  $\tau$ . As may be noticed, the correlation in the dataset is related to the non-stationary samples.

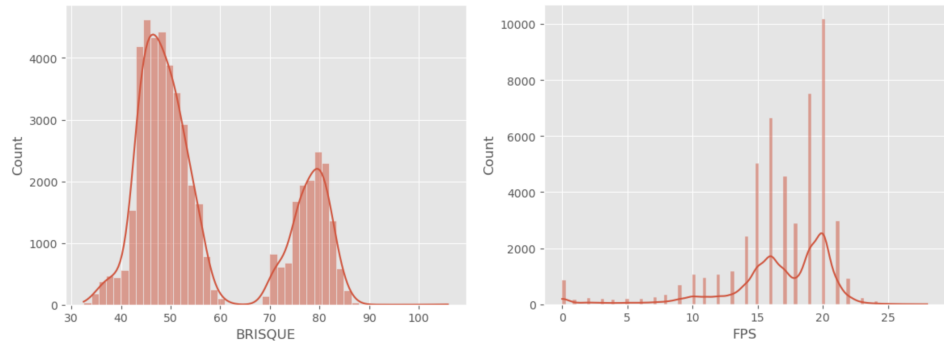


Figure 2: Distribution of the BRISQUE labels (left), and the FPS labels (right)

### 3.1.3 Stationarity

An auto-regressive (AR) process is a stochastic process who's output variable depends linearly on its own previous values, and some stochastic noise process, and may be described by the following relation

$$X_t = \sum_{\tau=1}^T \varphi_\tau X_{t-\tau} + \varepsilon_t \quad (1)$$

where  $\varphi_\tau$  represents the parameters of the model at time  $\tau$ ,  $X_{t-\tau}$  represents the output of the model in time  $t - \tau$ , and  $\varepsilon_t \sim N(0, \sigma^2)$ , i.e., a white noise process with zero mean and constant variance  $\sigma^2$ .

Stationarity refers to the degree to which a signal exhibits consistent statistical properties over time. Formally, a signal  $x_t$  is considered stationary if its distribution at time  $t$  is the same as its distribution at time  $t + \Delta t$  for any arbitrary offset  $\Delta t$ . This property is particularly important in our context, as stationary signals tend to contain recurring patterns that may hold strong predictive relevance.

To evaluate stationarity in our dataset, we applied the Augmented Dickey-Fuller (ADF) test, which assesses whether a model that represent a signal contains a unit root (an indication of non-stationarity).

The regular Dickey-Fuller (DF) [5] test is used as a test of stationarity in case of a simplified version of AR processes, where each future output depends only on an immediate previous output, or a first-order auto-regressive process, AR(1), or a Markovian process, and is described as

$$X_t = \rho X_{t-1} + \varepsilon_t \quad (2)$$

where  $X_t$  is the variable of interest in time  $t$ ,  $\rho$  is the coefficient and  $X_{t-1}$  is the value of the variable of interest in previous timestamp. In this simplified version of an AR process, we may test for the presence of a unit root by transforming eq. (2) to the following form:

$$X_t - X_{t-1} = \rho X_{t-1} + \varepsilon_t - X_{t-1} \quad (3)$$

$$\Delta X_t = (\rho - 1)X_{t-1} + \varepsilon_t = \delta X_{t-1} + \varepsilon_t \quad (4)$$

where  $\Delta$  represents the first difference operator,  $\delta \equiv \rho - 1$ . In case  $\rho = 1$  is a root of eq. (4), the model becomes dependent solely on the behavior of the  $\varepsilon_t \sim N(0, \sigma^2)$  term, i.e., non-stationary.

The DF test poses two hypotheses viz. the null hypothesis ( $H_0$ ) — a unit root is present in the sample, and the alternative hypothesis ( $H_1$ ) — the signal is stationary. The test rejects the null hypothesis if the statistic of the signal is smaller than the statistic that corresponds to one of confidence levels, viz. 1%, 5%, and 10% presented in table 3 [5].

The intuition behind the regular DF test is that if the process is stationary it should return to the mean value in the course of its advancement, i.e., large values should be followed by small and vice-a-versa. The constant return to the mean will make the current level of the series a significant predictor of the value in the next timestamp, and the null hypothesis will be rejected. On the other hand, if the small and large values occur with the same probability it means that the series is nonstationary, and we may not be able to dismiss the null hypothesis

Table 3: Dickey-Fuller table [5] for the stationarity test, where the null hypothesis ( $H_0$  = the series contain a unit root) is rejected in case the  $\tau$  statistic of the series is smaller than the critical value that corresponds to each of the confidence levels.

N	Confidence	1%	5%	10%
25	-3.724	-2.986	-2.633	
100	-3.498	-2.891	-2.582	
500	-3.434	-2.863	-2.568	

As the dependence of the next packet size only on the packet size of the last packet to arrived may not be asserted with a sufficient confidence, in our experiments we used the Augmented Dickey-Fuller (ADF) test, which differs from the DF test by addition of lag variables to the characteristic equation of the AR process as follows

$$\Delta X_t = \gamma X_{t-1} + \beta t + \alpha + \sum_{i=1}^L \delta y_{t-i} + \varepsilon_t \quad (5)$$

where  $\alpha$  is some constant,  $\beta$  the coefficient on a time trend, and  $L$  represents the lag order of the AR process (i.e., how big is the history that the next value of the process depends on). This formulation of the AR process allows

to consider higher order of AR models, and not just AR(1) and in the case of the regular DF test.

Intuitively, the ADF test states that if a process is characterized by a unit-root (i.e., nonstationary), then  $X_{t-1}$  should provide no new information regarding the changes in the next timestamp, thus we would conclude that  $\gamma = 0$ , and won't be able to reject  $H_0$ . On the other hand if the process has no unit root, the process will revert to the mean, i.e., the lagged level will provide relevant information for predicting the next change in the value, which will reject the  $H_0$ .

The results show that a majority of the samples (over 67%) satisfy the stationarity criterion. Given that our data reflects packet size fluctuations over time, which are driven by deterministic communications protocols, it is reasonable to assume that the dataset in its majority will exhibit stationary properties, i.e., constant mean and variance.

To visualize the signals better, we present an example of two distinct signals, viz. one stationary (red) and the other is non-stationary (blue), as presented in fig. 3 (left). From the figure we see that the non-stationary signal drops to 0 at the last 50 samples, while the stationary signal does not. This phenomenon may lay in the root for the reason that the dataset exhibits high correlation discussed in fig. 1 at the last 50 samples.

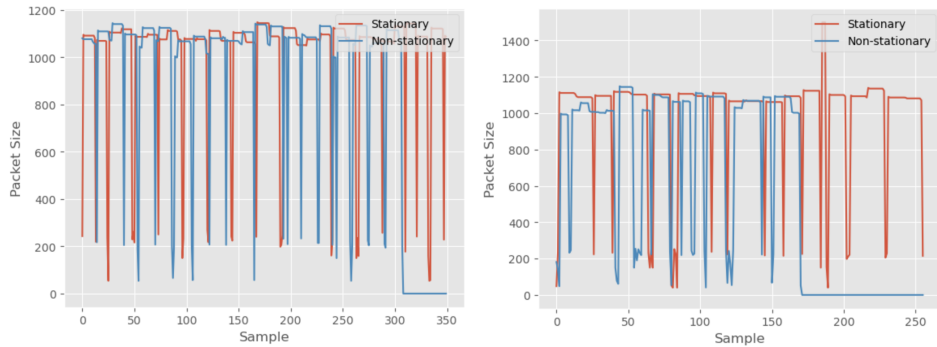


Figure 3: Two signals — one stationary (red) and another non-stationary (blue), on a full dataset (left) and on truncated dataset where the last 94 features were removed (right). From the figure we may note that the non-stationary signal drops to 0 value at the last 50 features, while the stationary signal remains high.

To test for this assumption, we have truncated the last 94 features, taking

only the first 256. Correlation table fig. 1 (right) of the truncated data appeared to include much less strong positively correlated features than in fig. 1 that resulted in a sharp raise in stationarity of the samples in the dataset from 67.3% to 87.1% (a raise of 19.8%), as show in fig. 4. Even after this manipulation a similar phenomenon was observed in the stationary and non-stationary signals, where the non-stationary signals included 0 at the end, as presented in fig. 3 (right), which supports our supposition expressed earlier, i.e. that the non-stationarity of the samples in our data results in a "tail" of 0's in the samples.

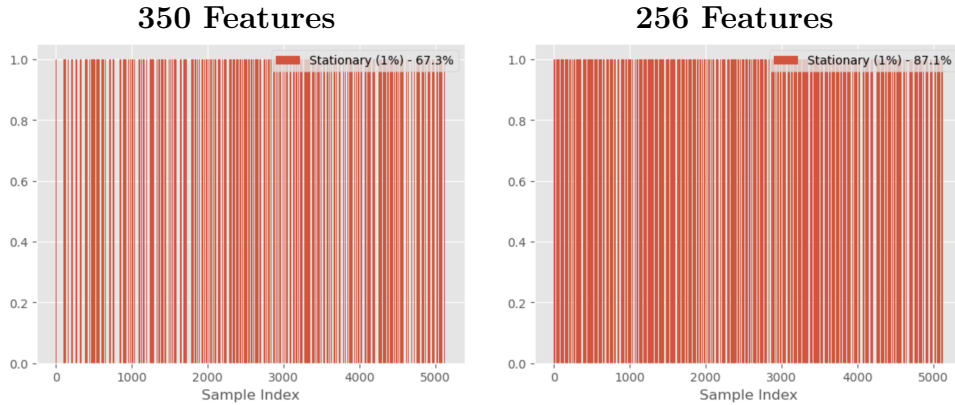


Figure 4: Visualization of the stationary vs nonstationary samples in the dataset with the highest confidence of 1%, as was described in table 3, where the red lines represent the stationary samples, while the gray nonstationary.

## 4 Methodology

In this chapter, we describe the proposed model and its components in detail. We also provide a brief overview of the underlying technologies that form the foundation of each module and offer motivation for their inclusion in the final architecture.

The model is composed of three modules: an Embedding module (EMBD), an Attention module (ATT), and a Convolutional Neural Network head module (CNN), as illustrated in fig. 5. The design draws partial inspiration from our previous work [27], in which we introduced a similar composite architecture built from an autoencoder and a convolutional network for tweet pre-

dition on the X social platform. In that earlier study, we relied exclusively on micro-level user activity features (namely, the presence (1) or absence (0) of a tweet at each timestamp), rather than on aggregated summary-statistics features. By representing these micro-level inputs as 2D matrices, which was shown to improve the non-linear ability of the network [37], and feeding them into a CNN-based head module, we were able to accurately predict future user interactions with high precision.

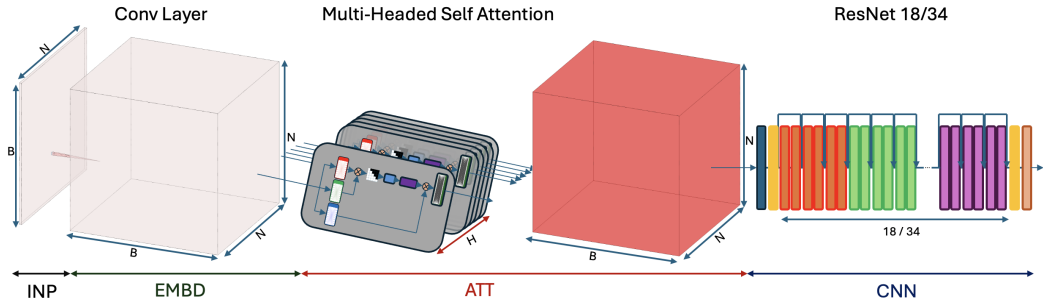


Figure 5: This figure demonstrates the qAttCNN module and its various components. a) The Embedding module that transforms the 1D input vector  $X_{1 \times N}$  into  $N \times N$  matrix. b) The self attention module, which attends to the most relevant features of the input embedded input vector represented as a 2D matrix (or an image). c) The CNN module that receives the 2D input matrix from the ATT module, and extracts local features from the image by convolution operation and pooling of the strongest features. This module is also responsible for the production of the final prediction

In the present research, we adopt the same general principle but introduce two significant modifications. First, instead of constructing 2D matrices by simply stacking the 1D input vectors (as done in our earlier work), we now employ dedicated Embedding (EMBD) and Attention (ATT) modules, which are jointly optimized during training to learn richer and more expressive representations of the input. Second, we replace the binary tweet/no-tweet activity indicators with the instantaneous sizes of data packets traversing the network.

## 4.1 Embedding Module (EMBD)

The EMBD module is implemented as a simple convolutional layer with  $1 \times 1$  kernel and output size equal to the data length  $N$ , as shown illustrated in fig. 6. Consequently, the output of this module is an  $N \times N$  tensor. In addition, this module serves as an initial filter for the data through the convolutional operation operation.

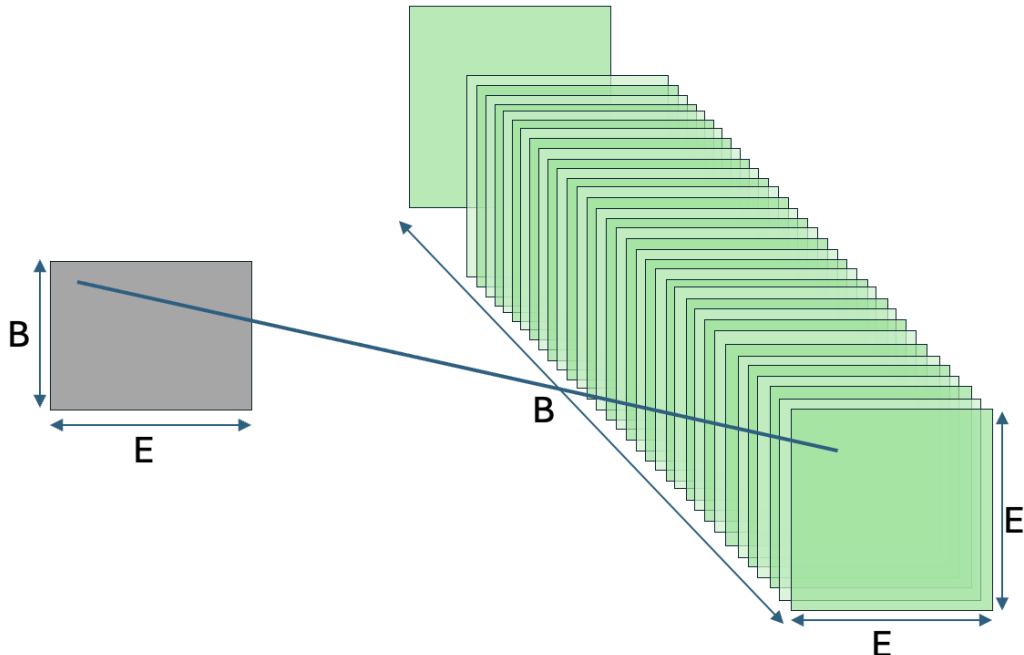


Figure 6: Embedding module that transforms a 1D data into 2D matrix

The core assumption, which is supported by substantial body of prior work [4, 25, 35, 24, 17, 1, 16, 11], is that the distinct protocols operating across the Internet give rise to identifiable low-level features within the data stream. These features typically exhibit characteristic patterns that can be reliably detected and associated with a target label, which in our case is the QoE metric. Because such patterns reflect structural properties of the traffic as a whole (for example, the TLS handshake establishing an encrypted end-to-end channel precedes any actual data transfer), the data must be represented in a form that preserves these dependencies.

As was shown in [27], an effective strategy is to transform the raw 1D measurements into a more structured 2D representation, enabling each sample to be interpreted in relation to its surrounding samples. As we hypothesize, this representation allows the model to capture meaningful segments of traffic behavior and subsequently map them to the corresponding QoE.

## 4.2 Multi-Head Self-Attention (MHSA) Module

This module receives the embedded data from the EMBED component in the form of keys ( $K$ ), queries ( $Q$ ), and values ( $V$ ), and reshapes them into an  $N \times N$  square matrix to serve as input to the CNN, as illustrated in fig. 7. Because the packet-arrival process is causal (i.e., it depends only on inputs from the present and past), we apply a mask to all outputs where  $j > i$ . This masking procedure, shown in the inset of fig. 7 and denoted by "Mask" operation, ensures that the model does not access future information.

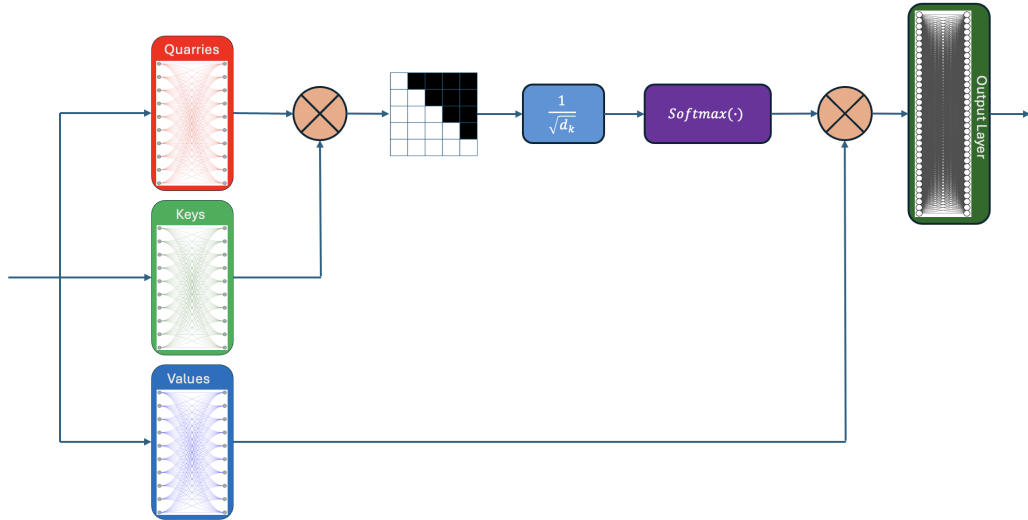


Figure 7: This figure presents the schematic representation of the self attention mechanism used in this model. This module returns output equal to the input size, i.e.  $N \times N$

Self-attention (SA) was first introduced unveiled its full potential the work by Vaswani et al. [34], as one of the major components in the Transformer architecture. This layer is designed to capture long-term relationship between

features, unlike the CNN which capture only the local features. It does that by weighting the features by multiplying them with the softmax of a scaled dot product of the same vectors, which results in the relative relevance of each of the features to the other. Particularly, the  $Softmax(\cdot)$  function is applied on the dot product of the Queries ( $Q$ ) and Keys ( $K$ ) scaled by the  $\sqrt{d_k}$  to ensure proper gradient flow, which results in weights of relevance of each feature to the other; then these weights are used to serve as a measure of feature relevance when they are multiplied by the Values ( $V$ ) term, as shown in eq. (6)

$$Z(K, Q, V) = Softmax\left(\frac{Q \cdot K^T}{\sqrt{d_K}}\right) \cdot V \quad (6)$$

As mentioned before, the  $\frac{1}{\sqrt{d_k}}$  term in the equation appears for gradient stability. If we assume that the input to the embedding layer  $X \sim N(0, 1)$  (standard normal distribution), the variance of each cell  $c_{ij}$  in the output matrix will be:

$$c_{ij} = Q_i \cdot K_j^T = \sum_{l=1}^{d_k} q_{il} k_{jl}^T \quad (7)$$

$$Var(c_{ij}) = Var\left(\sum_{l=1}^{d_k} q_{il} k_{jl}^T\right) = \sum_{l=1}^{d_k} Var(q_{il} k_{jl}^T) \quad (8)$$

but assuming  $Q, K \sim N(0, 1)$ , we get

$$Var(c_{ij}) = \sum_{l=1}^{d_k} Var(q_{il}) Var(k_{jl}^T) = \sum_{l=1}^{d_k} 1 = d_k \quad (9)$$

and the standard deviation of  $c_{ij}$  will be

$$\sigma(c_{ij}) = \sqrt{Var(c_{ij})} = \sqrt{d_k} \quad (10)$$

as the  $Softmax(\cdot)$  function is then applied on the  $Q \cdot K^T$ , and in case the  $d_k$  is very large, it may result in a vanishing gradients problem, and prevent the model from training.

### 4.3 Head Model

This module is responsible for the actual prediction generation based on features extracted from the transformed traffic input. It is represented by a convolutional neural network (CNN), head model (HM), and a fully connected layer as final prediction generator, that receives the flattened input from the last convolutional layer of the HM and outputs the final prediction, i.e., a number representing the QoE metric of interest as shown in fig. 8.

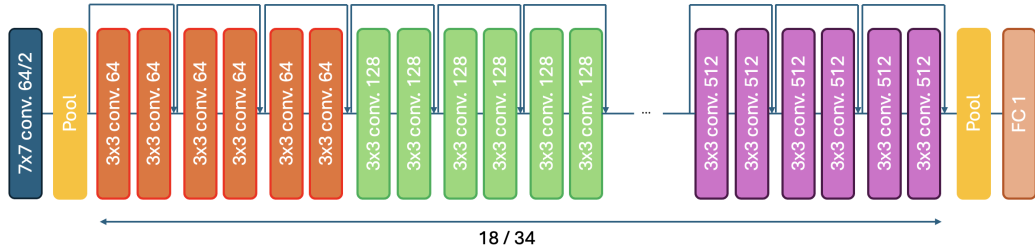


Figure 8: This figure demonstrates the CNN model head that is used for deep local feature extraction and final prediction

Convolutional neural networks (CNNs) were first introduced by LeCun et al. [13] and later gained significant popularity following the work of Krizhevsky et al. [12], which vividly demonstrated the potential of this architecture. CNNs are characterized by translation, rotation, and scale invariance, allowing them to capture the most representative features of the input. This property is particularly well suited for image-processing tasks, where objects may appear at different locations and scales within the frame yet should still be recognized as the same object.

In our experiments, translation invariance is the most important of these properties, as similar traffic behavior may appear in different regions of the data while corresponding to similar QoE measures. In our case, we apply a CNN head to  $Z_{N \times N}$ , i.e., the output of the ATT module, which contains the most relevant long-term features as described in section 4.2. By applying the CNN head, structural patterns in traffic are extracted and associated with appropriate label.

## 5 Experiments

### 5.1 Model Selection

To choose the best model for our experiments we have compared the final mean performance of different settings of the qAttCNN models, which varied by the head model used (viz. ResNet x18 / x35 / x50). As demonstrated in table 4, the best performance was reached by a qAttCNN model employing a ResNet35 head model. trained for 1000 epochs.

Table 4: In this table we present the comparison of the performance of the qAttCNN model evaluated with 10-fold CV with different head model architectures, viz. ResNet x16, x34, and x50. The metric used is Mean Absolute Error Percentage (MAEP) for two labels — BRISQUE, and FPS.

Architecture	BRISQUE	FPS
x18	$2.99 \pm 0.030$	<b><math>7.39 \pm 0.237</math></b>
x34	<b><math>2.14 \pm 0.025</math></b>	$9.09 \pm 0.279$
x50	$2.53 \pm 0.027$	$19.51 \pm 0.325$

Table 5: Computational Environment Parameters

Parameter	Model	Specification	Quantity
CPU	AMD Epic 9534	64 cores, 128 threads	2
RAM	DDR4	1 TB	1
GPU	Nvidia H100 NVL	94 GB	1

### 5.2 Evaluation Metric

The metric used for evaluation was chosen as a Mean Absolute Error Percentage (MAEP) described by eq. (11)

$$\varepsilon(t, p) = \frac{100}{N} \sum_{i=0}^N \left| 1 - \frac{p_i}{t_i} \right| \quad (11)$$

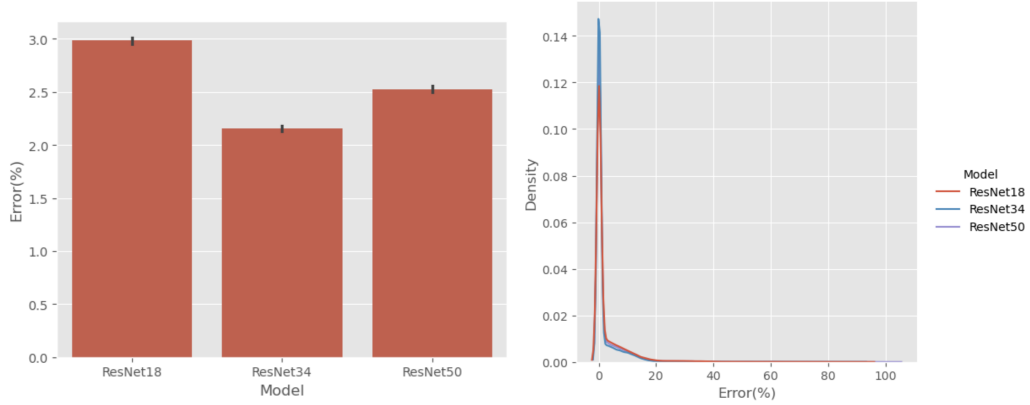


Figure 9: (Left) Mean errors for the BRISQUE QoE metric of different models achieved on the test sets in a 10-fold cross validation procedure (the lines represent the standard error). (Right) Distribution of the mean errors of different models.

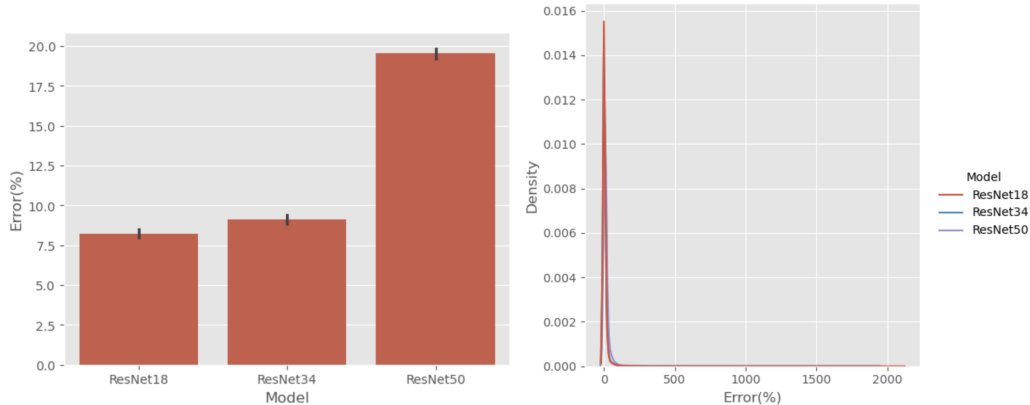


Figure 10: (Left) Mean errors for the FPS QoE metric of different models achieved on the test sets in a 10-fold cross validation procedure (the lines represent the standard error). (Right) Distribution of the mean errors of different models.

where  $N$  represents the number of data points in the vector. This metric may be interpreted as the scaleless prediction accuracy of the model, as the errors produced by the model in the course of the prediction are void of scale, and expressed in percentages with respect to the true label.

### 5.3 qAttCNN Training Procedure

#### 5.3.1 General Flow

The input signal is of length 350, representing the packet sizes or the inter-arrival times of the packets on the line, as was described in section 3. Prior to being passed through the SA module, the data was normalized, and transferred into frequency domain by the application of Fast Fourier Transform (FFT).

Then the transformed signal (only the real part) was passed into the MHSA module with 35 heads, which resulted in output shape  $B \times 350 \times 35$ , (where  $B$  is the batch size). The signal was transformed once more via an  $Conv_{1 \times 1}$  embedding layer, resulting in a square input shape of  $B \times 350 \times 350$ . The transferred signal was then passed through the head model (one of ResNet x18 / x35), outputting vectors of shape  $B \times 350$  that were passed through the final FC layer to generate the final predictions. The models were trained for 1000 epochs, and then tested on an unseen test set, which constituted 10% of the data. To ensure robust performance estimation, we employed a 10-fold cross validation technique in all our experiments, i.e., training the models on 90% of the dataset and testing on the remaining 10%, each time choosing different random, non-overlapping subset of the test data, and performing 10 such passes over the dataset.

#### 5.3.2 Pretrained Head Model Weights

In our experiments, we employed a transfer learning technique, where we used a pretrained model on ImageNet1k dataset, and freezing all the layers of the head model, except the final fully connected layer. In addition, the EMBD and the ATT modules were also trained, to locate most relevant features for to improve the predictions.

### 5.3.3 Learning Rate

We took inspiration from the work of L. N. Smith [30] who proposed a cyclical learning rate (LR) schedule to counter the problem of local minima in models based on neural networks. In this technique, the learning rate is modified with some period  $P$ , in the end of which the value is restored to the initial state, as shown in eq. (12).

$$l(t_0 + P) = l(t_0) \quad (12)$$

In our case, we started with a relatively high learning rate of  $5 \times 10^{-3}$  (which is a commonly used value for LR in applications using Adam optimizer), and decreased it periodically with a period of  $P = 4$ , each period spanning over 50 epochs; in the first 3 50-epoch chunks the LR was decreased by  $10^{-4}$ , while in the last 50 epochs of a period the LR was decreased by a factor of 0.9 each 10 epochs (5 times in total).

At the beginning of a new round  $r_t$  (where  $t = 4 \cdot 50k = 200k$ ), the initial LR was not restored to the initial LR as in round  $r_{t-1}$ , but to the LR of the second period of the 50 epochs (LR decreased by  $10^{-4}$ ) relative to the LR value of the first epoch range, as shown in fig. 11 (left). This technique provided both slow convergence closer to the end of the training, and the ability to escape local minima, as in the original work.

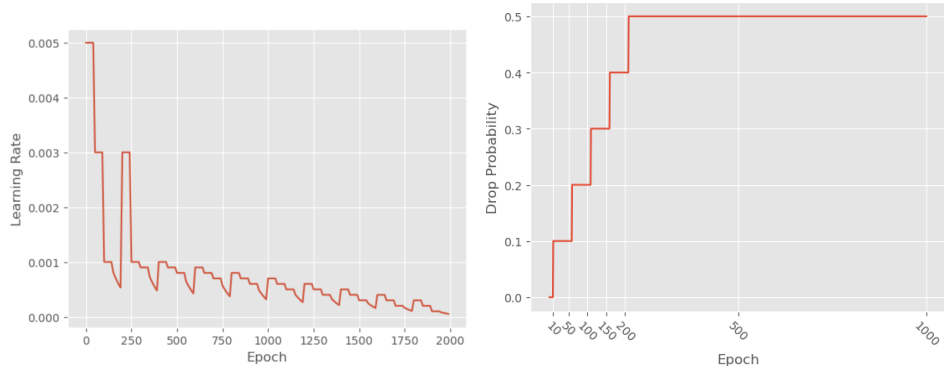


Figure 11: Left - Proposed version of a cyclical LR used in this work. The LR value is gradually decreased over the course of training, with spikes to the high learning rates to escape local minima traps. Right - The schedule employed during the training in the Drop Out layer of the model

### 5.3.4 Regularization

To avoid overfitting, we employed two regularization techniques, viz. Dropout [31] technique on the last FC layer, and data augmentation. Similarly to the learning rate, we employed a schedule for the dropout as well, where we increased the drop probability  $p$  by 0.1 each 50 epochs until it reached its maximal value of 0.5, after which it stayed constant till the end of the training process (until epoch 1000 in our case); an illustration of this procedure is shown in fig. 11 (right).

As for the augmentation we used a simple additive noise  $N \sim (0, 1)$  and a row shuffle technique. The augmentations were applied based on two randomly chosen thresholds, viz.  $n \in [0, 1]$  and  $s \in [0, 1]$ , where the former was chosen in range [0-0.3] and the latter in range [0-0.4]. Then, another random variable  $p \in [0, 1]$  was chosen for each of the augmentations as a specific probability for the augmentation to be applied.

### 5.3.5 Loss Function

In our experiments we used a custom loss function, that was designed to follow the final evaluation metric we used in our previous studies [28, 29] to assess its predictive potential, i.e., the Mean Average Error Percentage (MAEP) (which was discussed latter in section 5.2). The loss function used for the qAttCNN and the two versions of the QoENet1D was defined as described in eq. (13).

$$\mathcal{L}(l, x) = \frac{100}{B} \cdot \sum_{i=1}^B \left| 1 - \frac{x_i}{l_i} \right| \quad (13)$$

## 5.4 Ablation Study

In this section we present the results for the ablation we performed to test for the significance of different modules of the qAttCNN model, viz. the EMBD, FFT, ATT, CNN. In each experiment, we changed the normal use of each of the modules whether by excluding it entirely (as in the case of the FFT, ATT and CNN modules) or by changing its functionality (as in the case of the EMBD module, which in the proposed model is frozen, so in the course of the ablation, we trained the weights of this module to test for the influence of this procedure). In addition, we tested the influence of the correlation in

the features highlighted in section 3.1.1 by evaluating the performance of the qAttCNN on a subset of the original dataset, that was acquired by truncating the correlated features. All the experiments were performed using a 10-fold CV procedure, and the final results are presented in section 5.4 (for detailed scatter plots of the predicted vs the true values produced by the models see fig. 17 and fig. 18). An error distribution for each of the models with ablated modules is presented in fig. 14 and in fig. 15.

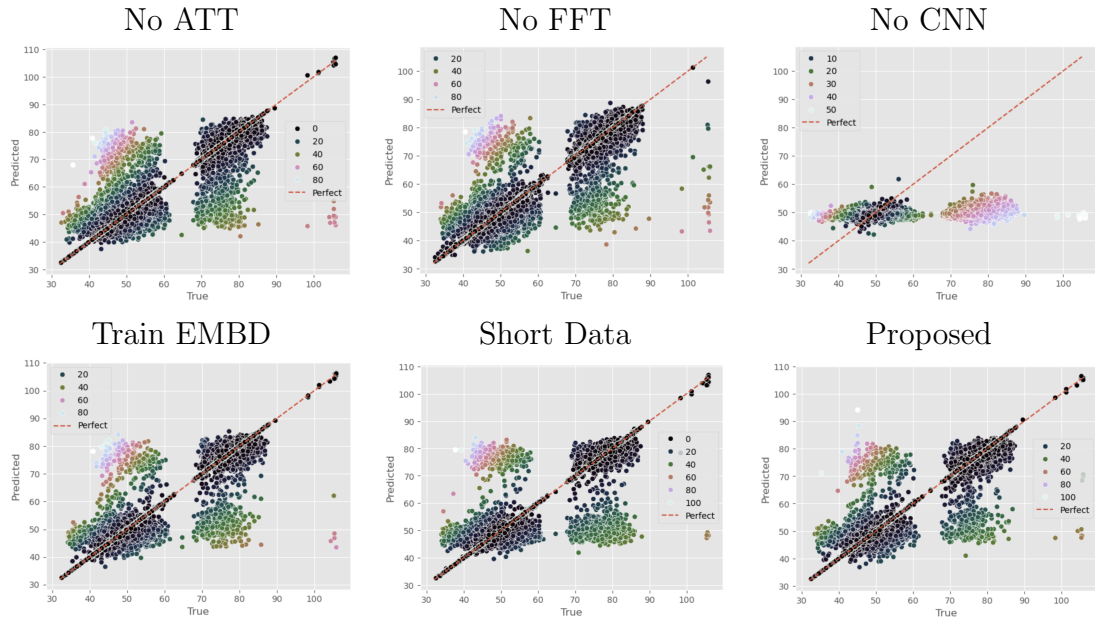


Figure 12: Predicted vs real BRISQUE value in the course of the ablation study

## 5.5 Reference Models Training Procedure

### 5.5.1 Classical ML Models

These models were trained and tested on two separate datasets, in a 10-fold CV technique. During the training phase the data in the train dataset was fitted, and latter predictions were generated for the unseen test data. These were compared with the metric described in eq. (11).

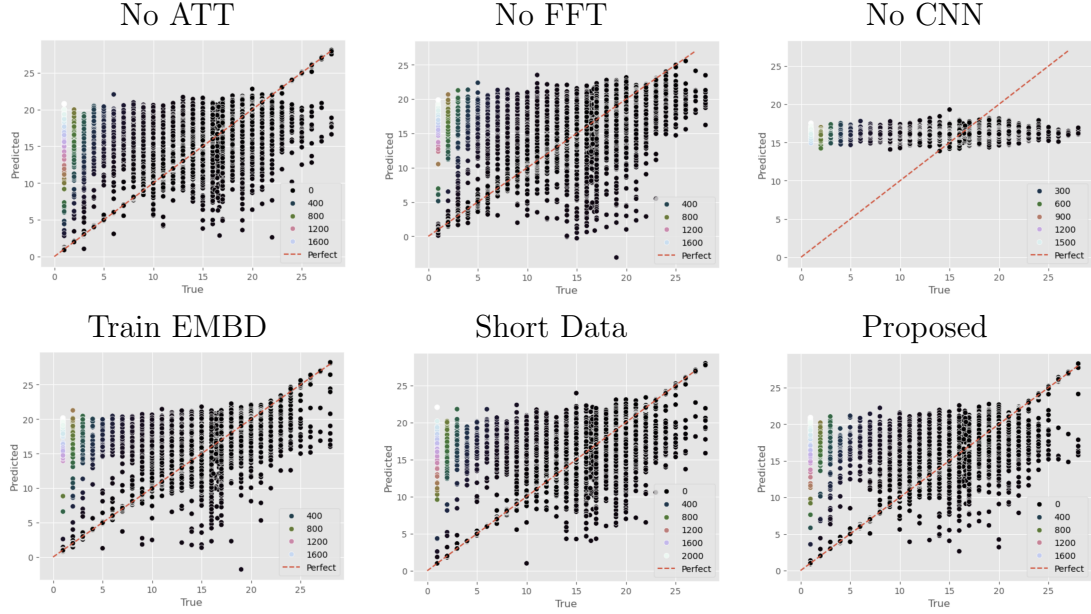


Figure 13: Predicted vs real FPS value in the course of the ablation study

Table 6: The results for the ablation study conducted on the qAttCNNx34 for the BRISQUE, and the qAttCNNx18 for the FPS models. We ablated each of the models' components, and conducted a 10 CV to test for robust performance indication

Module	BRISQUE	FPS
Train EMBD	$2.16 \pm 0.026$	$8.24 \pm 0.280$
Short Data	$2.88 \pm 0.026$	$9.72 \pm 0.276$
Without FFT	$2.47 \pm 0.026$	$11.07 \pm 0.256$
Without ATT	$2.90 \pm 0.029$	$10.58 \pm 0.292$
Without CNN	$16.34 \pm 0.062$	$28.16 \pm 0.027$
Proposed	<b><math>2.14 \pm 0.025</math></b>	<b><math>7.39 \pm 0.237</math></b>

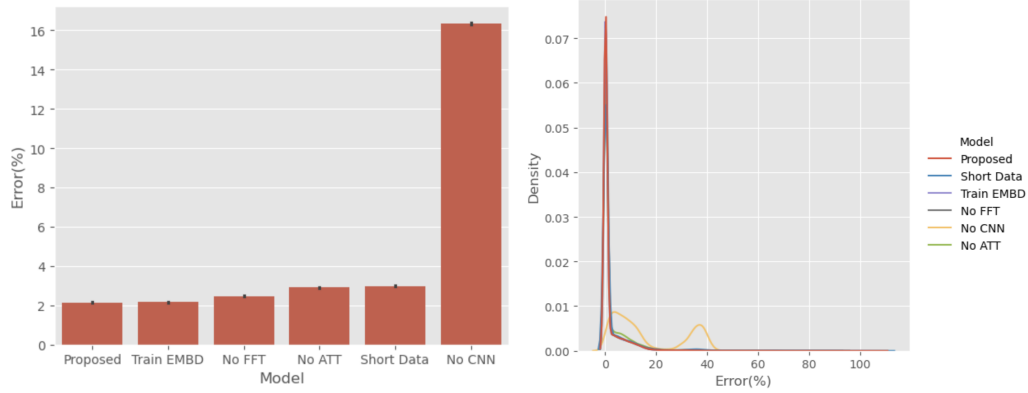


Figure 14: (Left) Mean errors for the BRISQUE QoE metric of different models with ablated modules, to test their importance to the overall performance, achieved on the test sets in a 10-fold cross validation procedure (the lines represent the standard error). (Right) Distribution of the mean errors of the ablated models.

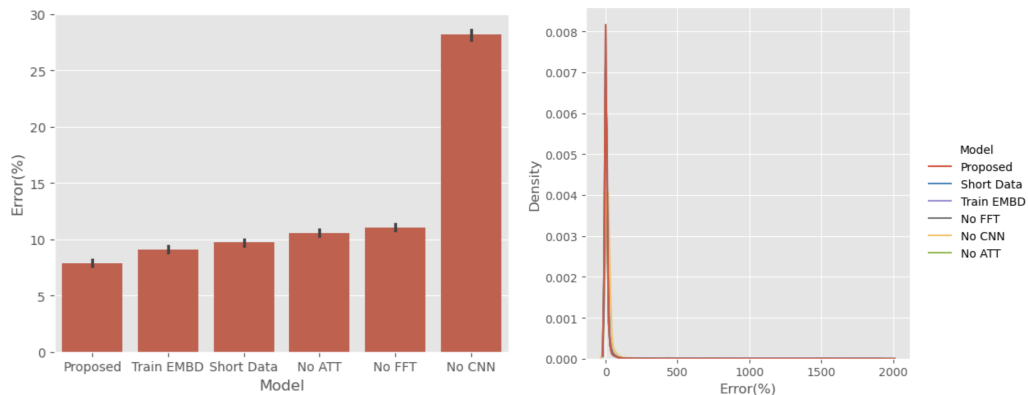


Figure 15: (Left) Mean errors for the FPS QoE metric of different models with ablated modules, to test their importance to the overall performance, achieved on the test sets in a 10-fold cross validation procedure (the lines represent the standard error). (Right) Distribution of the mean errors of the ablated models.

## 6 Results

In this section we present the mean prediction results for the test set of each of the models, and averaged over 10-folds of the 10-fold CV procedure. The results for qAttCNN and QoENet1D models are calculated by loading the best-performing model (in terms of loss, as described in section 5.3.5) on each fold and testing on this fold’s test set. In table 7 we summarize the final results of all the models used in our experiments.

Table 7: In this table we show the final performance of the proposed model (qAttCNN), and 8 other models that are usually used in prediction of QoE in encrypted traffic viz. Linear Regression (LR), Support Vector Machine (SVM), Adaptive Boosting (AdaBoost), eXtreeme Gradient Boosting (XGBoost), Categorical Boosting (CatBoost), Random Forest (RF), and QoENet1D [28], predicting two QoE metrics — BRISQUE and FPS (The standard deviation is presented in brackets).

Model	BRISQUE	FPS
Linear Regression	$9.20 \pm 0.042$	$24.27 \pm 0.414$
SVM	$8.06 \pm 0.042$	$22.61 \pm 0.441$
AdaBoost	$15.9 \pm 0.042$	$37.11 \pm 0.296$
XGBoost	$7.01 \pm 0.032$	$18.50 \pm 0.303$
CatBoost	$7.35 \pm 0.032$	$19.64 \pm 0.326$
Random Forest	$5.54 \pm 0.030$	$15.80 \pm 0.297$
QoENet1D-Basic	$2.94 \pm 0.025$	$10.93 \pm 0.301$
QoENet1D-Optimized	$2.61 \pm 0.026$	$10.36 \pm 0.288$
qAttCNN(x18)	$2.99 \pm 0.030$	<b><math>7.39 \pm 0.237</math></b>
qAttCNN(x34)	<b><math>2.14 \pm 0.025</math></b>	$9.10 \pm 0.280$

We report that both for the BRISQUE, and the FPS metrics qAttCNN model provided the best results. Nevertheless it should be noted that the best performing model for the two metrics did not agree on the head model used in their architecture — ResNet34 for BRISQUE and ResNet18 for FPS. We conjecture that this phenomenon may be explained by the nature of the predicted label (i.e. continuous for BRISQUE, and discreet in the case of FPS). As the discreet labels have less information due to quantization, deeper models might have a greater risk for overfitting the data. On the other

hand the shallowness of the smaller head model, may have acted as another regularization factor, providing an incentive for the model to generalize rather than remember seen examples.

To visualize better the results, we have plotted the mean error percentage of each model and for each of the QoE metrics for all the test sets used in the course of the CV, which presented in fig. 16 (for detailed scatter plots of the predicted vs true values see fig. 17 and fig. 18). From these figures we see that the proposed model achieves the best results in the MAPE on both of the QoE metrics, and strongly outperforms the RF model, which is the standard model used in the task of tabular data.

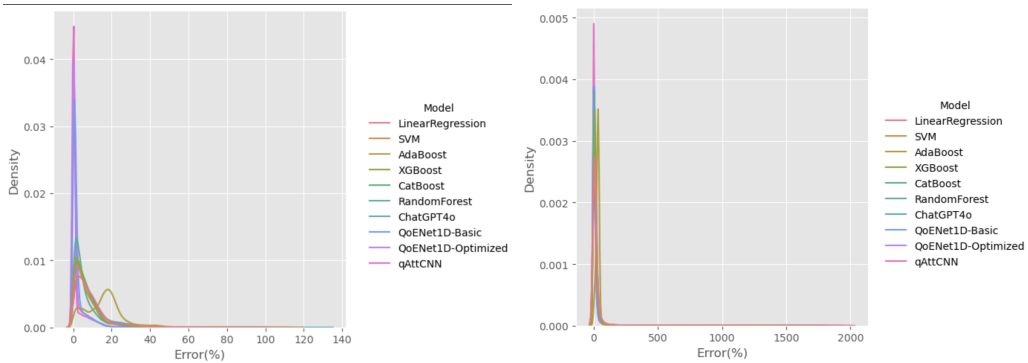


Figure 16: This plot presents the final mean test results for BRISQUE and FPS prediction, expressed in error percentage, over 10-fold cross validation

## 7 Conclusions and Future Work

In current work we presented a novel architecture, which we call the qAttCNN, that is based on self attention mechanism as a global feature finder, and CNN as local feature extractor, for QoE prediction under the constraint of encrypted traffic communication. We showed that the qAttCNN outperforms all the models usually used for QoE prediction. We also proposed an improved training setting for the QoENet1D DNN architecture proposed by us in the past, that achieved slightly worse results than the qAttCNN, but having a big advantage in training time over the qAttCNN. For the limitations of our work we want to designate the long training time of the qAttCNN, and the dependence on large data of both qAttCNN and the QoENet1D.

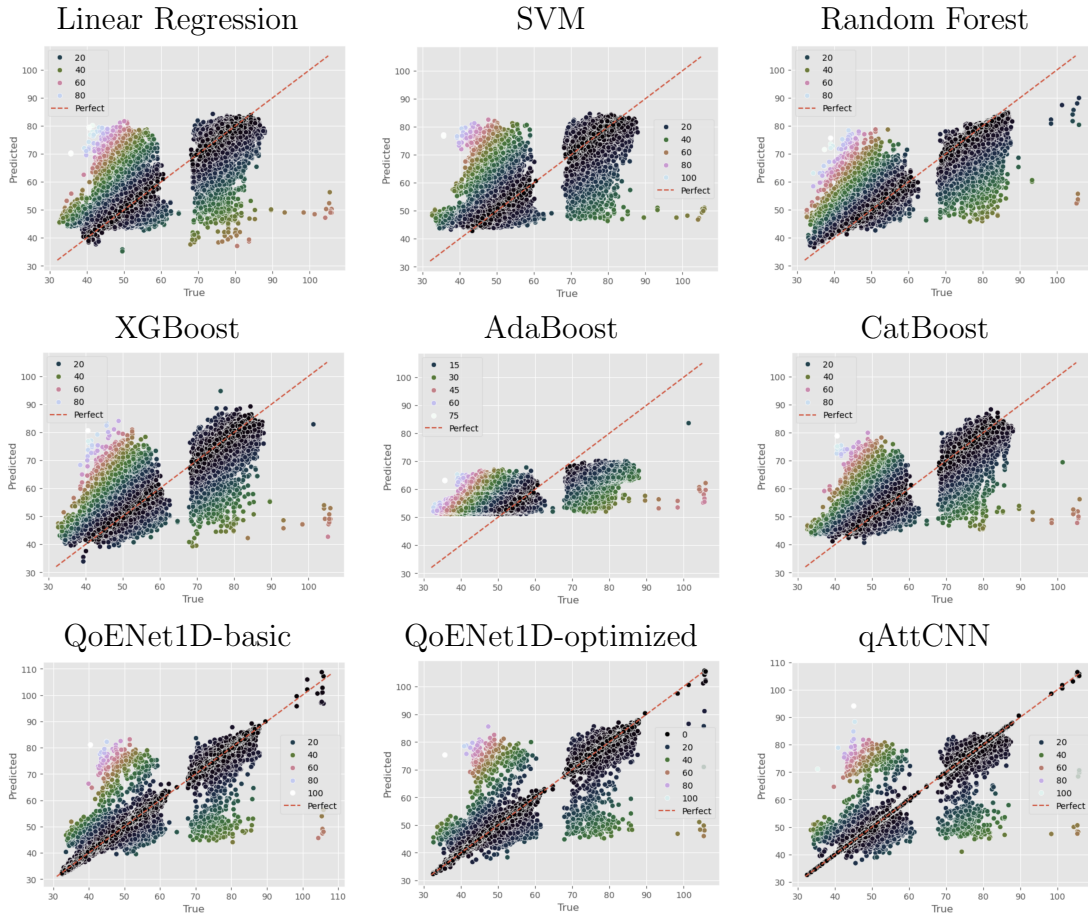


Figure 17: Predicted vs real BRISQUE value predicted by each of the best-performing models over the test sets of each of the 10-fold CV

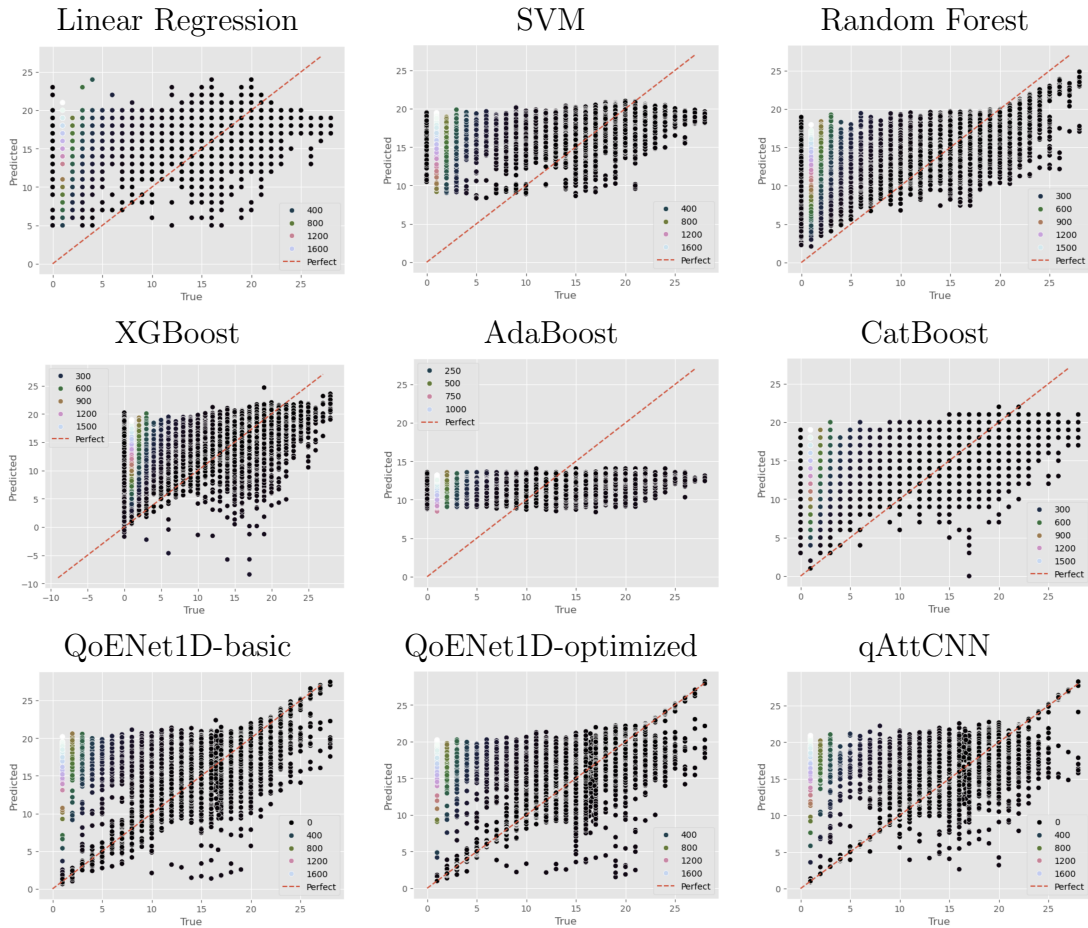


Figure 18: Predicted vs real FPS value produced by each of the best-performing models over the test sets of each of the 10-fold CV

Another limitation of our method is its lack of generality, as our data was collected only on a single platform. We designate this aspect for future work. Another direction for future research on this topic may be testing the model with different head module architectures, e.g., ResNext, FstrRCNN, etc.

## References

- [1] Giuseppe Aceto et al. “Mobile encrypted traffic classification using deep learning”. In: *2018 Network traffic measurement and analysis conference (TMA)*. IEEE. 2018, pp. 1–8.
- [2] Abdelhak Bentaleb et al. “Bandwidth prediction in low-latency chunked streaming”. In: *Proceedings of the 29th ACM workshop on network and operating systems support for digital audio and video*. 2019, pp. 7–13.
- [3] Francesco Bronzino et al. “Inferring streaming video quality from encrypted traffic: Practical models and deployment experience”. In: *Proceedings of the ACM on Measurement and Analysis of Computing Systems* 3.3 (2019), pp. 1–25.
- [4] Zhitang Chen et al. “Seq2img: A sequence-to-image based approach towards ip traffic classification using convolutional neural networks”. In: *2017 IEEE International conference on big data (big data)*. IEEE. 2017, pp. 1271–1276.
- [5] David A Dickey and Wayne A Fuller. “Distribution of the estimators for autoregressive time series with a unit root”. In: *Journal of the American statistical association* 74.366a (1979), pp. 427–431.
- [6] Giorgos Dimopoulos et al. “Measuring video QoE from encrypted traffic”. In: *Proceedings of the 2016 Internet Measurement Conference*. 2016, pp. 513–526.
- [7] Alexey Dosovitskiy. “An image is worth 16x16 words: Transformers for image recognition at scale”. In: *arXiv preprint arXiv:2010.11929* (2020).
- [8] Nick Feamster and Jennifer Rexford. “Why (and how) networks should run themselves”. In: *arXiv preprint arXiv:1710.11583* (2017).
- [9] Craig Gutterman et al. “Requet: Real-time QoE detection for encrypted YouTube traffic”. In: *Proceedings of the 10th ACM Multimedia Systems Conference*. 2019, pp. 48–59.
- [10] Geoffrey E Hinton and Ruslan R Salakhutdinov. “Reducing the dimensionality of data with neural networks”. In: *science* 313.5786 (2006), pp. 504–507.

- [11] Jonas Höchst et al. “Unsupervised traffic flow classification using a neural autoencoder”. In: *2017 IEEE 42Nd Conference on local computer networks (LCN)*. IEEE. 2017, pp. 523–526.
- [12] Alex Krizhevsky, Ilya Sutskever, and Geoffrey E Hinton. “Imagenet classification with deep convolutional neural networks”. In: *Advances in neural information processing systems* 25 (2012).
- [13] Yann LeCun et al. “Backpropagation applied to handwritten zip code recognition”. In: *Neural computation* 1.4 (1989), pp. 541–551.
- [14] Haijun Liu et al. “TEC Prediction Based on Att-CNN-BiLSTM”. In: *IEEE Access* 12 (2024), pp. 68471–68484.
- [15] Xiaohu Liu et al. “Prediction of carbon emissions in Zhejiang province based on ATT-CNN-LSTM model”. In: *2023 8th Asia Conference on Power and Electrical Engineering (ACPEE)*. IEEE. 2023, pp. 1918–1922.
- [16] Manuel Lopez-Martin et al. “Network traffic classifier with convolutional and recurrent neural networks for Internet of Things”. In: *IEEE access* 5 (2017), pp. 18042–18050.
- [17] Mohammad Lotfollahi et al. “Deep packet: A novel approach for encrypted traffic classification using deep learning”. In: *Soft Computing* 24.3 (2020), pp. 1999–2012.
- [18] Hongzi Mao, Ravi Netravali, and Mohammad Alizadeh. “Neural adaptive video streaming with pensieve”. In: *Proceedings of the conference of the ACM special interest group on data communication*. 2017, pp. 197–210.
- [19] David Naylor et al. “The cost of the” s” in https”. In: *Proceedings of the 10th ACM International on Conference on emerging Networking Experiments and Technologies*. 2014, pp. 133–140.
- [20] Irena Orsolic et al. “A machine learning approach to classifying YouTube QoE based on encrypted network traffic”. In: *Multimedia tools and applications* 76.21 (2017), pp. 22267–22301.
- [21] Junki Oura et al. “Qoe estimation method with time-series features extracted from packet flows for video streaming”. In: *2024 IEEE 21st Consumer Communications & Networking Conference (CCNC)*. IEEE. 2024, pp. 1–6.

- [22] Andriy Panchenko et al. “Website Fingerprinting at Internet Scale.” In: *NDSS*. Vol. 1. 2016, p. 23477.
- [23] Dario Raca et al. “On leveraging machine and deep learning for throughput prediction in cellular networks: Design, performance, and challenges”. In: *IEEE Communications Magazine* 58.3 (2020), pp. 11–17.
- [24] Shahbaz Rezaei and Xin Liu. “Deep learning for encrypted traffic classification: An overview”. In: *arXiv preprint arXiv:1810.07906* (2018).
- [25] Shahbaz Rezaei and Xin Liu. “How to achieve high classification accuracy with just a few labels: A semi-supervised approach using sampled packets”. In: *arXiv preprint arXiv:1812.09761* (2018).
- [26] Meng Shen et al. “DeepQoE: Real-time measurement of video QoE from encrypted traffic with deep learning”. In: *2020 IEEE/ACM 28th International Symposium on Quality of Service (IWQoS)*. IEEE. 2020, pp. 1–10.
- [27] Michael Sidorov, Ofer Hadar, and Dan Vilenchik. “Revisiting information cascades in online social networks”. In: *Mathematics* 13.1 (2024), p. 77.
- [28] Michael Sidorov et al. “Estimating QoE from Encrypted Video Conferencing Traffic”. In: *Sensors (Basel, Switzerland)* 25.4 (2025), p. 1009.
- [29] Michael Sidorov et al. “Reliable QoE Prediction in IMVCAs Using an LMM-Based Agent”. In: *Sensors* 25.14 (2025), p. 4450.
- [30] Leslie N Smith. “Cyclical learning rates for training neural networks”. In: *2017 IEEE winter conference on applications of computer vision (WACV)*. IEEE. 2017, pp. 464–472.
- [31] Nitish Srivastava et al. “Dropout: a simple way to prevent neural networks from overfitting”. In: *The journal of machine learning research* 15.1 (2014), pp. 1929–1958.
- [32] Jun Tang et al. “An ionospheric TEC forecasting model based on a CNN-LSTM-attention mechanism neural network”. In: *Remote Sensing* 14.10 (2022), p. 2433.
- [33] Maria Torres Vega, Decebal Constantin Mocanu, and Antonio Liotta. “Unsupervised deep learning for real-time assessment of video streaming services”. In: *Multimedia Tools and Applications* 76.21 (2017), pp. 22303–22327.

- [34] Ashish Vaswani et al. “Attention is all you need”. In: *Advances in neural information processing systems* 30 (2017).
- [35] Ly Vu, Cong Thanh Bui, and Quang Uy Nguyen. “A deep learning based method for handling imbalanced problem in network traffic classification”. In: *Proceedings of the 8th international symposium on information and communication technology*. 2017, pp. 333–339.
- [36] Bin Yi et al. “Process Quality Prediction Algorithm of Multi output Workshop Based on ATT-CNN-TCN”. In: *Proceedings of the 2023 6th International Conference on Machine Vision and Applications*. 2023, pp. 120–127.
- [37] Jiahui Yu et al. “Wide activation for efficient and accurate image super-resolution”. In: *arXiv preprint arXiv:1808.08718* (2018).
- [38] Hongcheng Zhao et al. “Electricity Price Prediction in Electricity Markets Using an ATT-CNN-LSTM Model Based on the Sparrow Search Algorithm”. In: *2024 3rd Asia Power and Electrical Technology Conference (APET)*. IEEE. 2024, pp. 589–594.